Supporting Information for:

Nanocomposite ruthenium oxide electrocatalysts for the low-pH oxygen evolution reaction

Mohamed R. Rizk[1], Zhiyuan Wang[1], Darcy Simondson[1], Tam D. Nguyen[1], Douglas R. MacFarlane[1], Rosalie K. Hocking[2], Alexandr N. Simonov[1]*

[1] School of Chemistry, Monash University, Victoria 3800, Australia
[2] Department of Chemistry and Biotechnology, Swinburne University of Technology.

* Corresponding author: alexandr.simonov@monash.edu

TABLE OF CONTENTS

SUPPLEMENTARY FIGURES

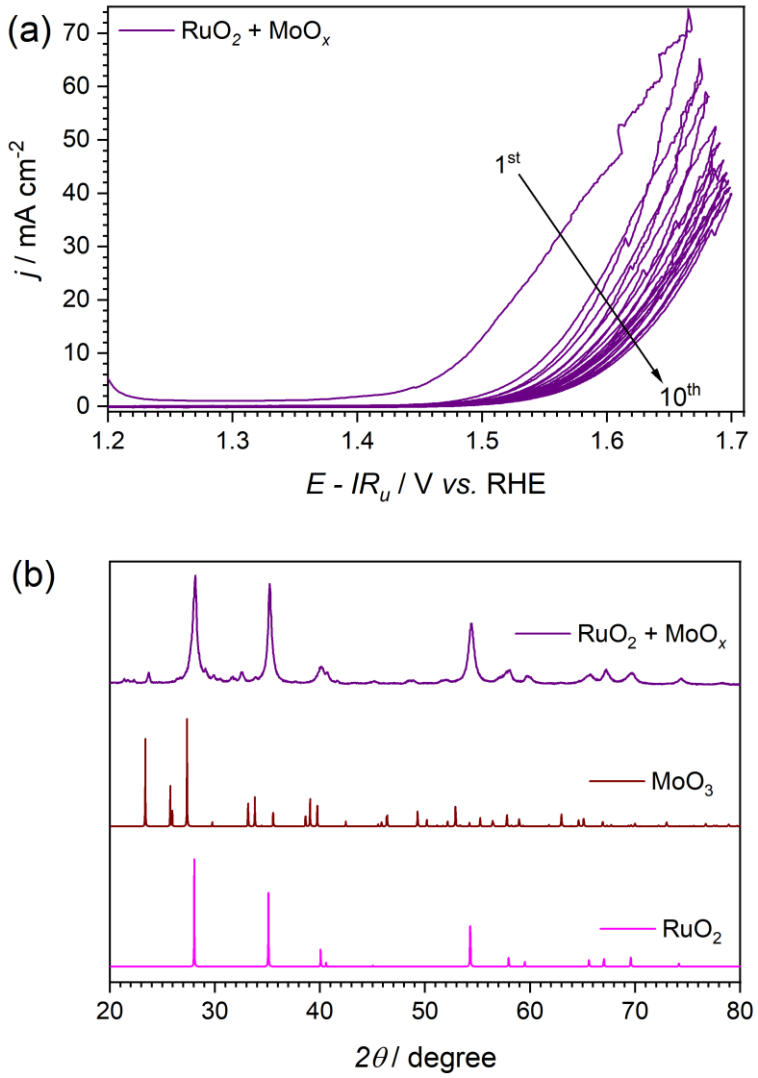

Figure S1. Initial OER performance and XRD pattern of a material prepared by direct coprecipitation of Ru and Mo hydroxides followed by calcination at 600 °C.

(a) Cyclic voltammograms (scan rate, v = 0.010 V s^{-1}; ten consecutive scans) recorded for a GC electrode functionalised with 0.25 mg cm^{-2} of the material in O_2-saturated, stirred (600 rpm) 0.5 M H_2SO_4 at 23 ± 2 °C. Currents are normalised to the geometric surface area of the electrode (0.20 cm^2); potentials were post-corrected for ohmic losses. (b) X-ray diffraction pattern of the catalyst highlighting the peaks corresponding to the RuO_2 (COD 1000058) and MoO_3 (COD 1011073) phas

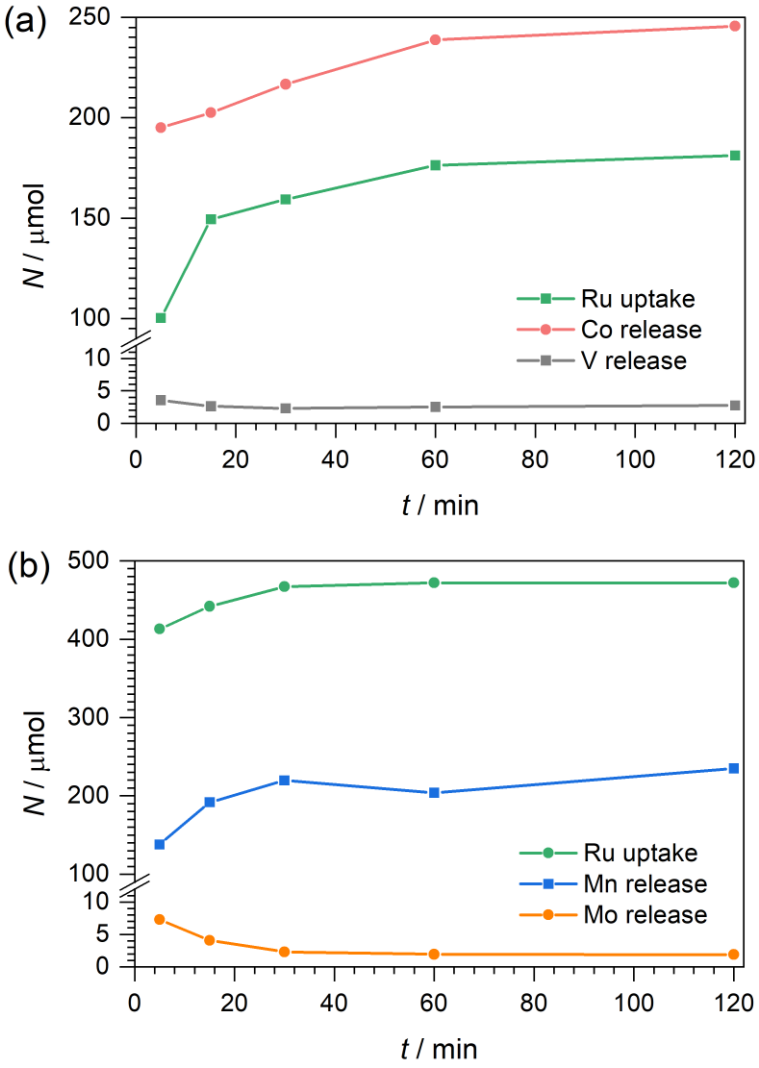

Figure S2. Uptake of Ru^{3+} and release of the LDH constituent metal ions into the solution.

Data are shown in terms of absolute amount of dissolved Ru^{3+} removed from the solution (*green*), and Co (*red*), Mn (*blue*), V (*grey*) and Mo (*orange*) released into the solution during the reaction between (a) 307 µmol $RuCl_3$ with 260 µmol CoV-LDH, and (b) 511 µmol $RuCl_3$ with 290 µmol MnMo-LDH in 50 mL water at 23 ± 2 °C. Lines are guides to the eye.

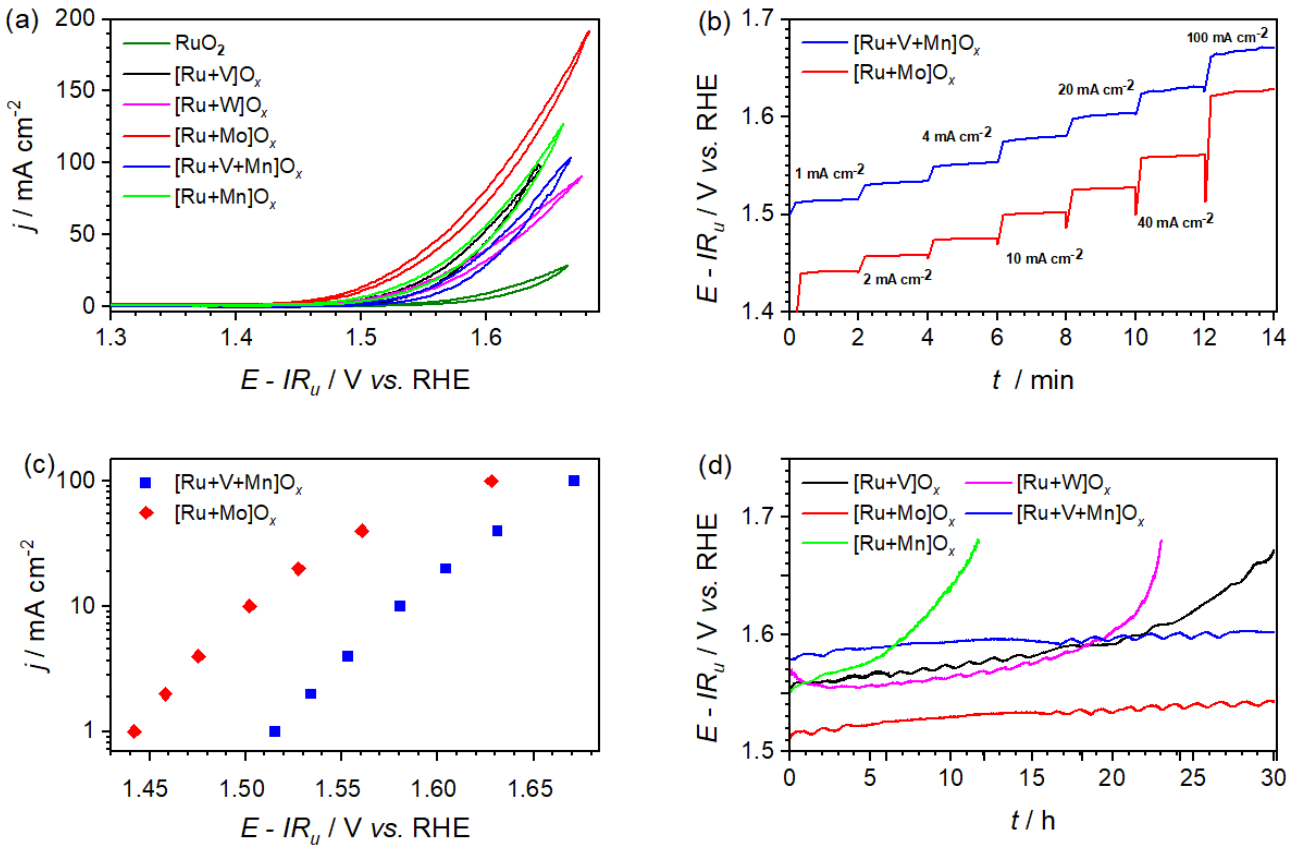

Figure S3. OER performance of the RuO_2 composites with various metal oxides.

(a) Cyclic voltammograms (v = 0.010 V s^{-1}; 5th quasi-stabilised scans) recorded for catalysts defined in the figure. (b) Chronopotentiograms at varied current densities (see figure), and (c) corresponding OER polarisation plots for $[Ru+V+Mn]O_x$ (*blue*) and $[Ru+Mo]O_x$ (*red*). (d) Extended chronopotentiograms at 10 mA cm^{-2} for different catalysts (see figure). Experiments were undertaken using a Pt/Ti electrode functionalised with 0.25 mg cm^{-2} of a catalyst in O_2-saturated, stirred (600 rpm) 0.5 M H_2SO_4 at 23 ± 2 °C. Currents are normalised to the geometric surface area of the electrode (0.25 cm^2); potentials were post-corrected for ohmic losses.

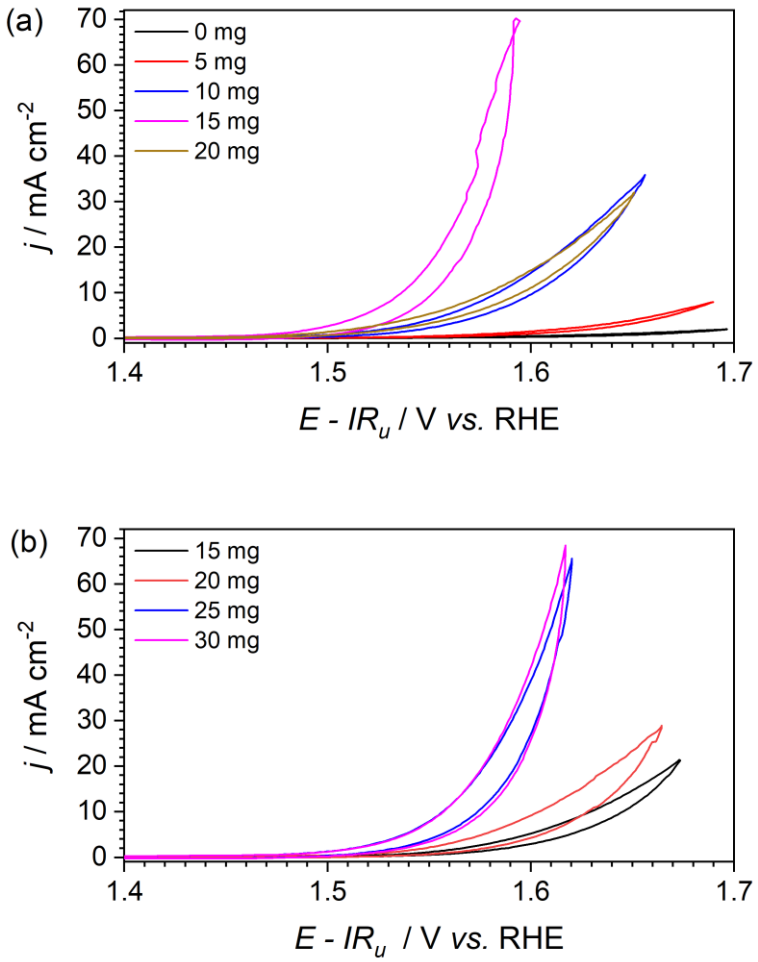

Figure S4. Optimisation of the $RuCl_3$ amount used for the synthesis of the V-based catalysts. Cyclic voltammograms (v = 0.010 V s^{-1}; 5th quasi-stabilised scans) recorded for a GC electrode functionalised with 0.25 mg cm^{-2} of (a) [Ru+V]O_x and (b) [Ru+Mn+V]O_x prepared using different amounts of $RuCl_3$ during the ion-exchange step (**Figure 1**; main text). Experiments were undertaken in O_2-saturated, stirred (600 rpm) 0.5 M H_2SO_4 at 23 ± 2 °C. Currents are normalised to the geometric surface area of the electrode (0.20 cm^2); potentials were post-corrected for the ohmic losses.

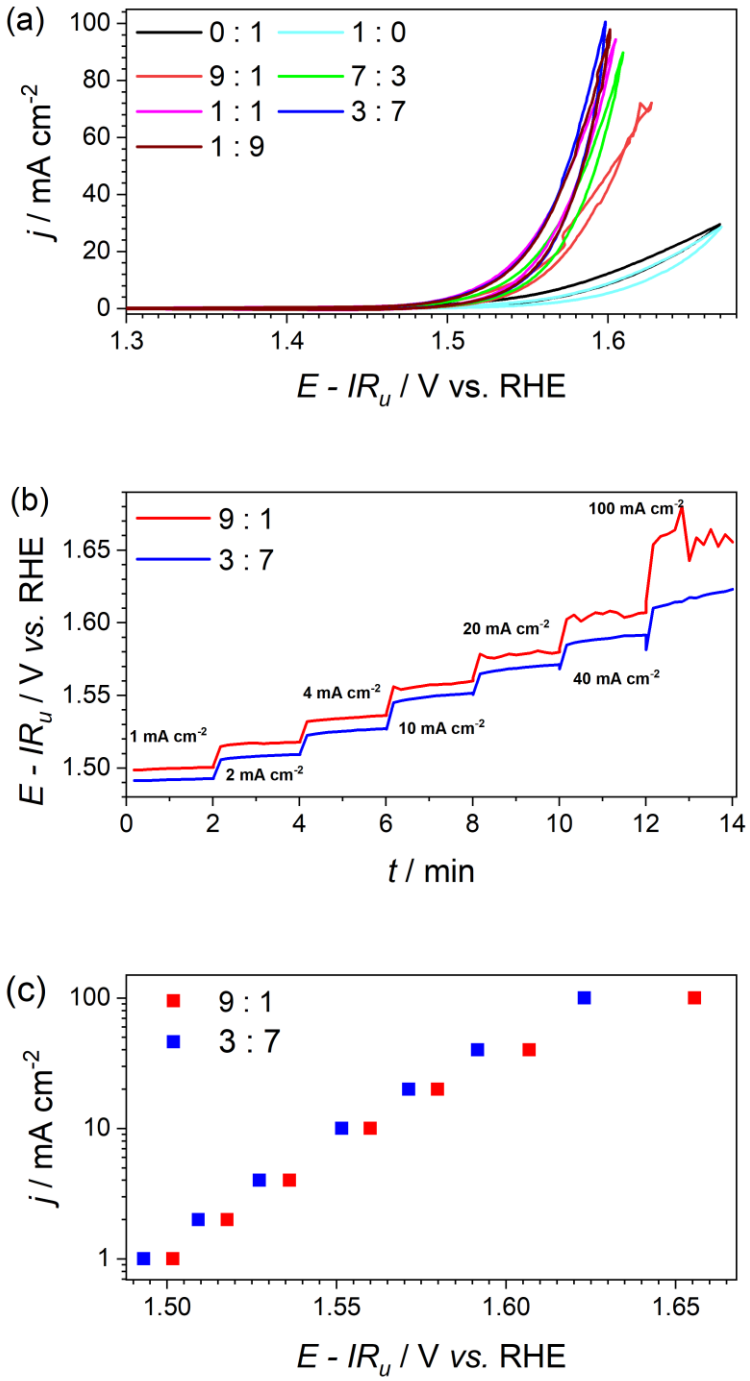

Figure S5. Optimisation of the Co to V ratio for [Ru+V]O_x.

(a) Cyclic voltammograms (v = 0.010 V s^{-1}; 5th quasi-stabilised scans), (b) chronopotentiograms at different current densities (see figure), and (c) corresponding OER polarisation plots for the [Ru+V]O_x catalysts synthesised using different Co : V atomic ratio (see figure). Data were obtained using a GC electrode functionalised with 0.25 mg cm^{-2} of a catalyst in O_2-saturated, stirred (600 rpm) 0.5 M H_2SO_4 at 23 ± 2 °C. Currents are normalised to the geometric surface area of the electrode (0.20 cm^2); potentials were post-corrected for ohmic losses.

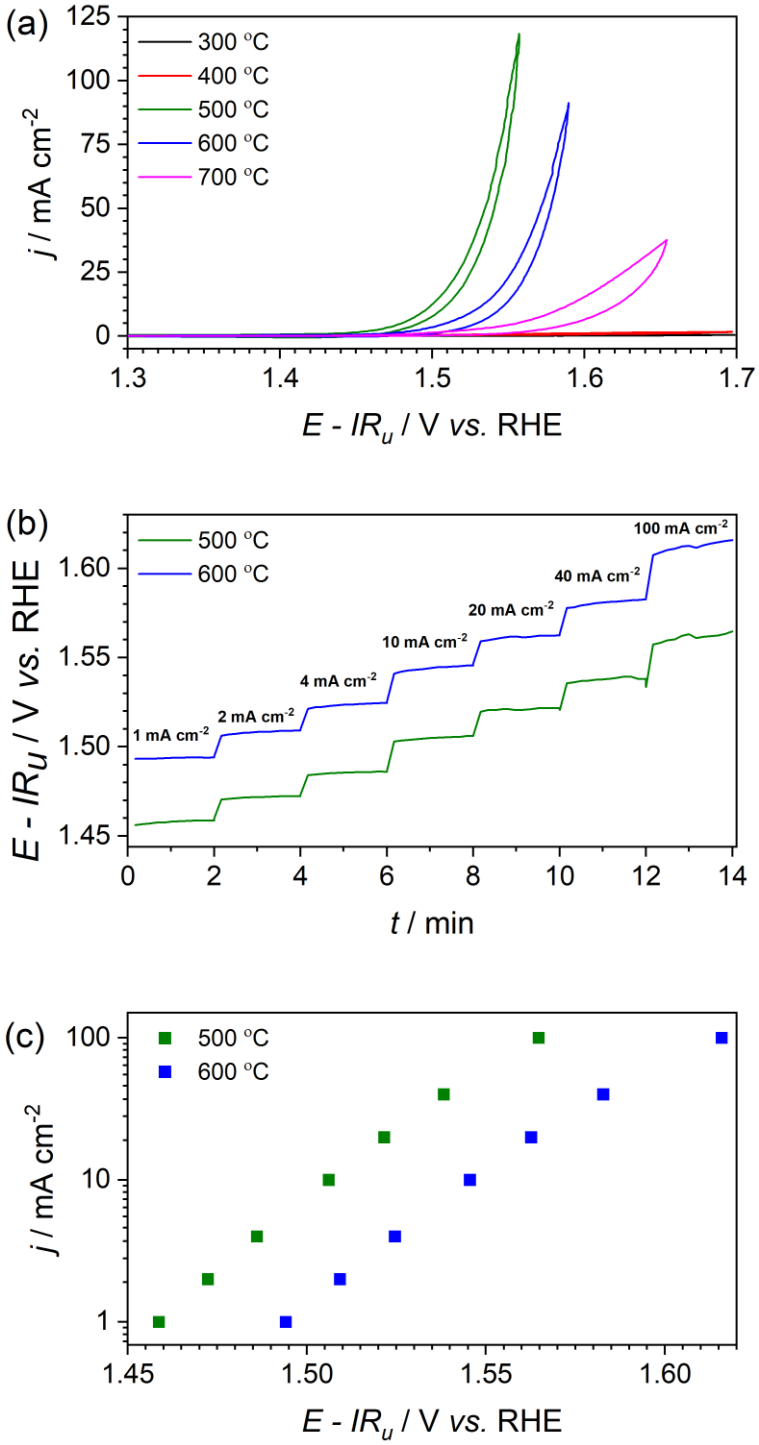

Figure S6. Optimisation of the calcination temperature for [Ru+V]O_x.

(a) Cyclic voltammograms (v = 0.010 V s^{-1}; 5th quasi-stabilised scans), (b) chronopotentiograms at different current densities (see figure), and (c) corresponding OER polarisation plots for the [Ru+V]O_x catalysts calcined at different temperatures (see figure). Data were obtained using a GC electrode functionalised with 0.25 mg cm^{-2} of a catalyst in O_2-saturated, stirred (600 rpm) 0.5 M H_2SO_4 at 23 ± 2 °C. Currents are normalised to the geometric surface area of the electrode (0.20 cm^2); potentials were post-corrected for ohmic losses.

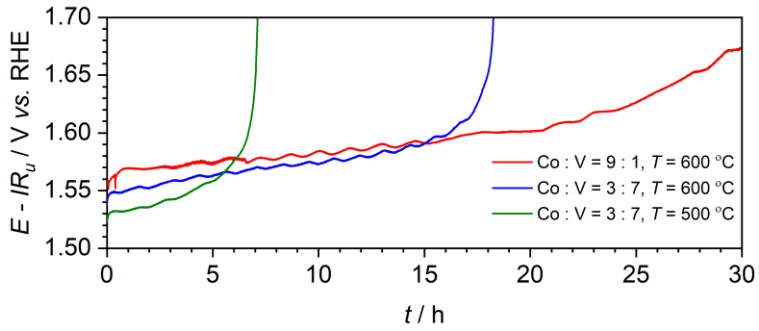

Figure S7. Stability of the [Ru+V]O_x catalysts.

Extended chronopotentiograms recorded at 10 mA cm^{-2} (per geometric surface area of the electrode; 0.25 cm^2) for Pt/Ti electrodes functionalised with 0.25 mg cm^{-2} of [Ru+V]O_x catalysts prepared using different Co : V atomic ratios and calcination temperatures shown in the figure. Experiments were undertaken in O_2-saturated, stirred (600 rpm) 0.5 M H_2SO_4 at 23 ± 2 °C. Potentials were post-corrected for ohmic losses.

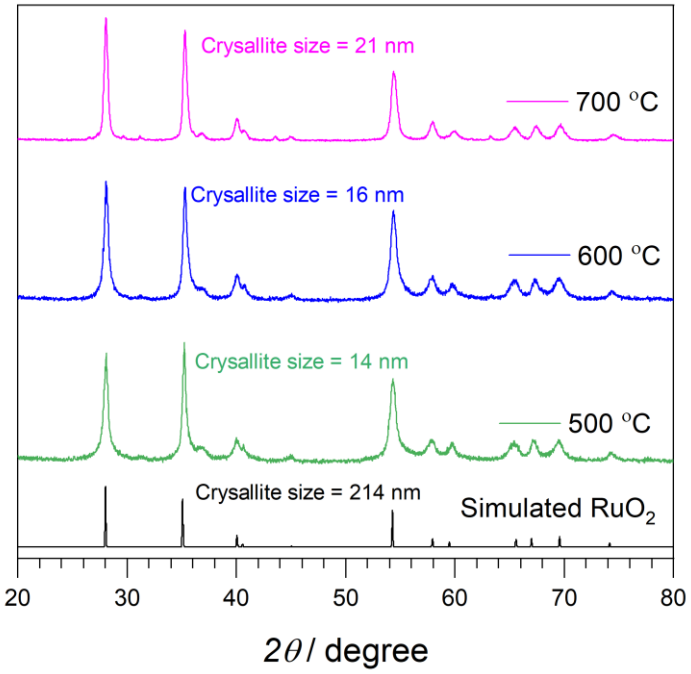

Figure S8. XRD patterns of [Ru+V]O_x calcined at different temperatures.
Data for [Ru+V]O_x calcined at 500 °C (*green*), 600 °C (*blue*), and 700 °C (*pink*) are compared to the simulated pattern for the RuO_2 reference (*black*; COD 1000058 with a crystallite size of 214 nm).

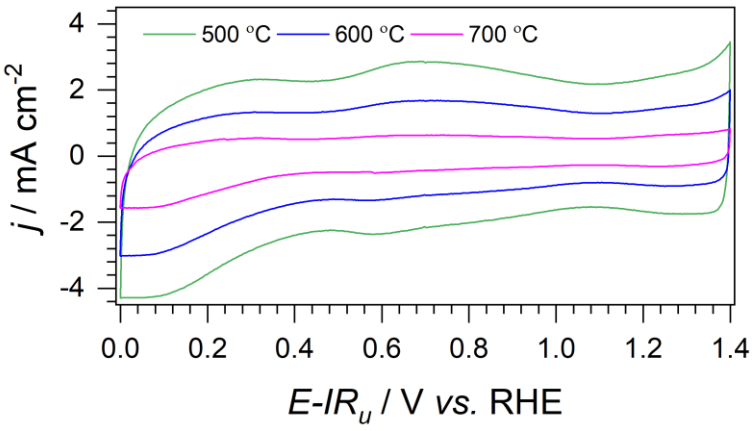

Figure S9. Cyclic voltammetry of [Ru+V]O_x calcined at different temperatures.
Cyclic voltammograms (scan rate, v = 0.050 V s^{-1}; 5th scans) for [Ru+V]O_x calcined at 500 °C (*green*), 600 °C (*blue*), and 700 °C (*pink*). Experiments were undertaken in O_2-saturated and continuously stirred (600 rpm) 0.5 M H_2SO_4. Catalysts were immobilised on glassy carbon (0.20 cm^2) electrodes at a loading of 0.25 mg cm^{-2}. Currents are normalised to the geometric surface area of the electrodes. Potentials were manually corrected for ohmic losses after measurements.

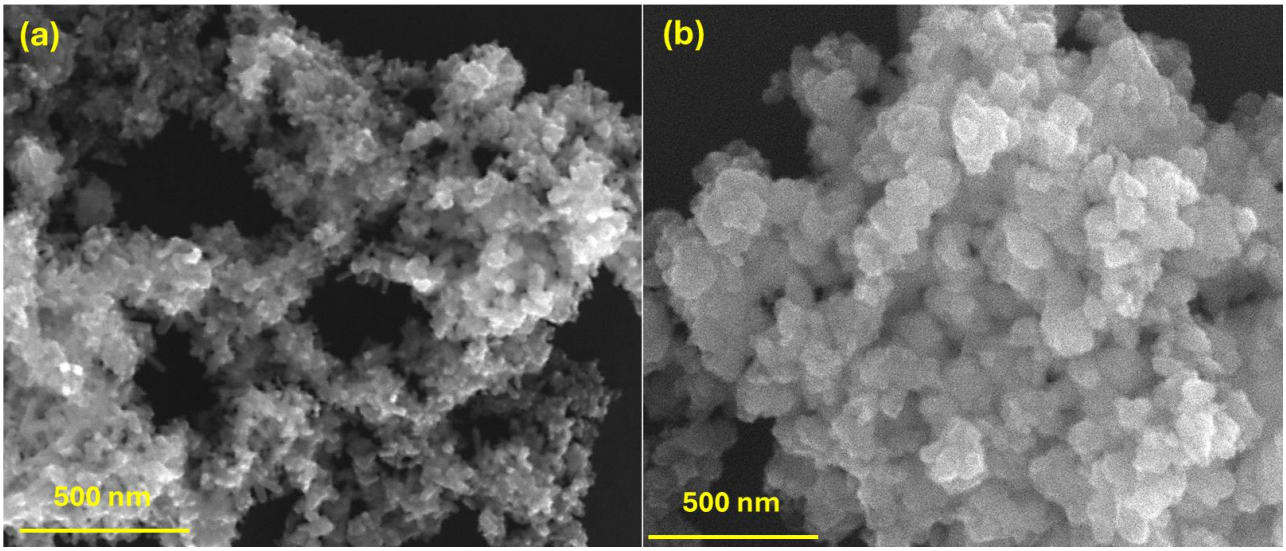

Figure S10. SEM analysis of (a) [Ru+Mn]O_x and (b) [Ru+Mo]O_x.

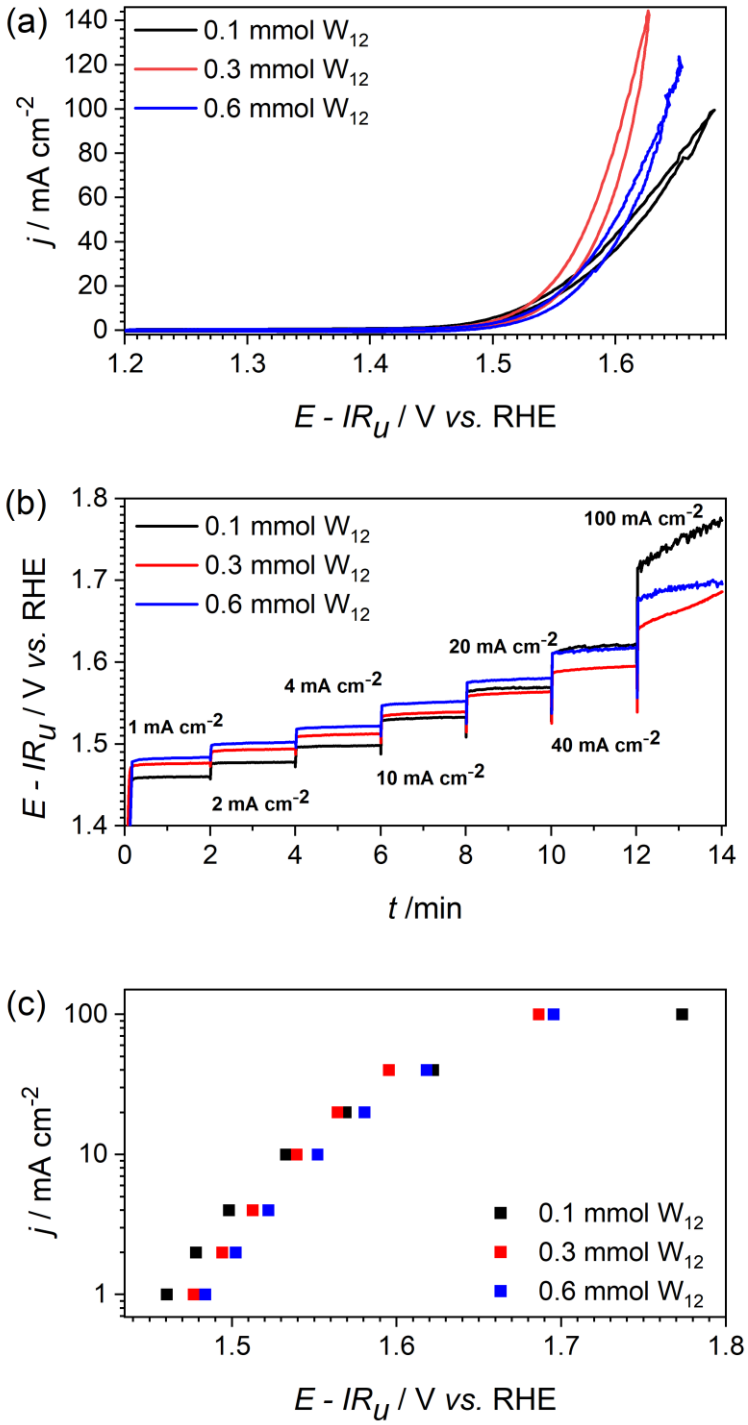

Figure S11. Optimisation of the tungsten content used for the synthesis of [Ru+W]O_x.
(a) Cyclic voltammograms (v = 0.010 V s^{-1}; 5th quasi-stabilised scans), (b) chronopotentiograms at different current densities (see figure), and (c) corresponding OER polarisation plots for the [Ru+W]O_x catalysts synthesised using different amounts of $(NH_4)_{10}H_2(W_2O_7)_6$ (see figure). Data were obtained using a GC electrode functionalised with 0.25 mg cm^{-2} of a catalyst in O_2-saturated, stirred (600 rpm) 0.5 M H_2SO_4 at 23 ± 2 °C. Currents are normalised to the geometric surface area of the electrode (0.20 cm^2); potentials were post-corrected for ohmic losses.

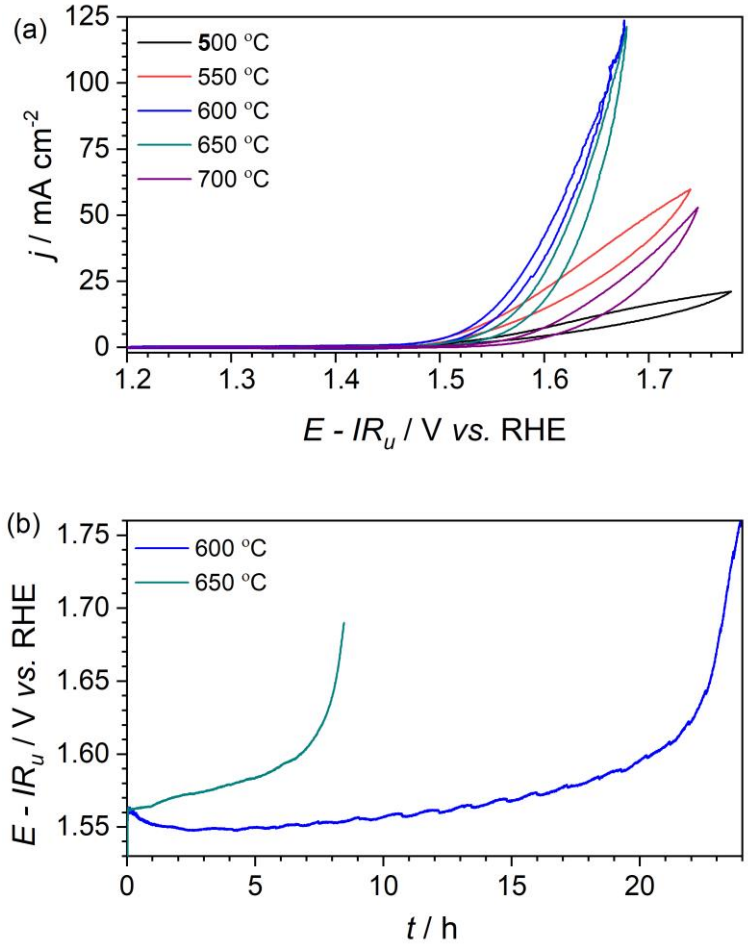

Figure S12. Optimisation of the calcination temperature for [Ru+W]O_x.

(a) Cyclic voltammograms (v = 0.010 V s^{-1}; 5th quasi-stabilised scans), (b) chronopotentiograms at different current densities (see figure), and (c) corresponding OER polarisation plots for the [Ru+W]O_x catalysts calcined at different temperatures (see figure). Data were obtained using a GC electrode functionalised with 0.25 mg cm^{-2} of a catalyst in O_2-saturated, stirred (600 rpm) 0.5 M H_2SO_4 at 23 ± 2 °C. Currents are normalised to the geometric surface area of the electrode (0.20 cm^2); potentials were post-corrected for ohmic losses.

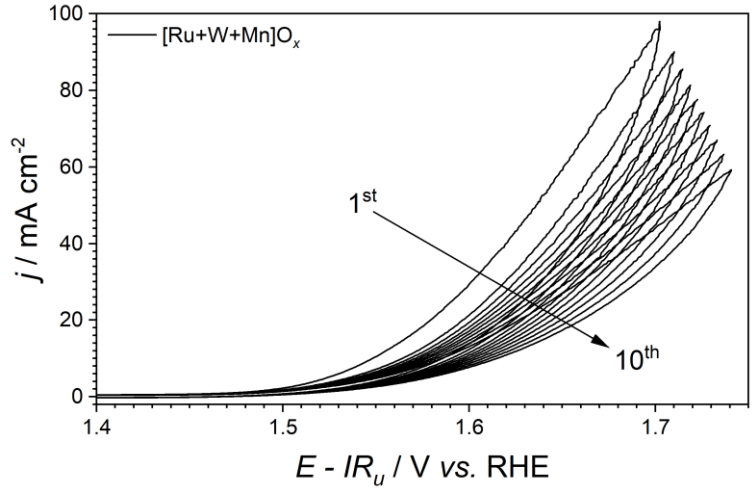

Figure S13. Initial OER performance of [Ru+W+Mn]O$_x$.

Cyclic voltammograms (v = 0.010 V s^{-1}; 10 consecutive scans) recorded for a GC electrode functionalised with 0.25 mg cm^{-2} of [Ru+W+Mn]O$_x$ in O_2-saturated, stirred (600 rpm) 0.5 M H_2SO_4 at 23 ± 2 °C. Currents are normalised to the geometric surface area of the electrode (0.20 cm^2); potentials were post-corrected for ohmic losses.

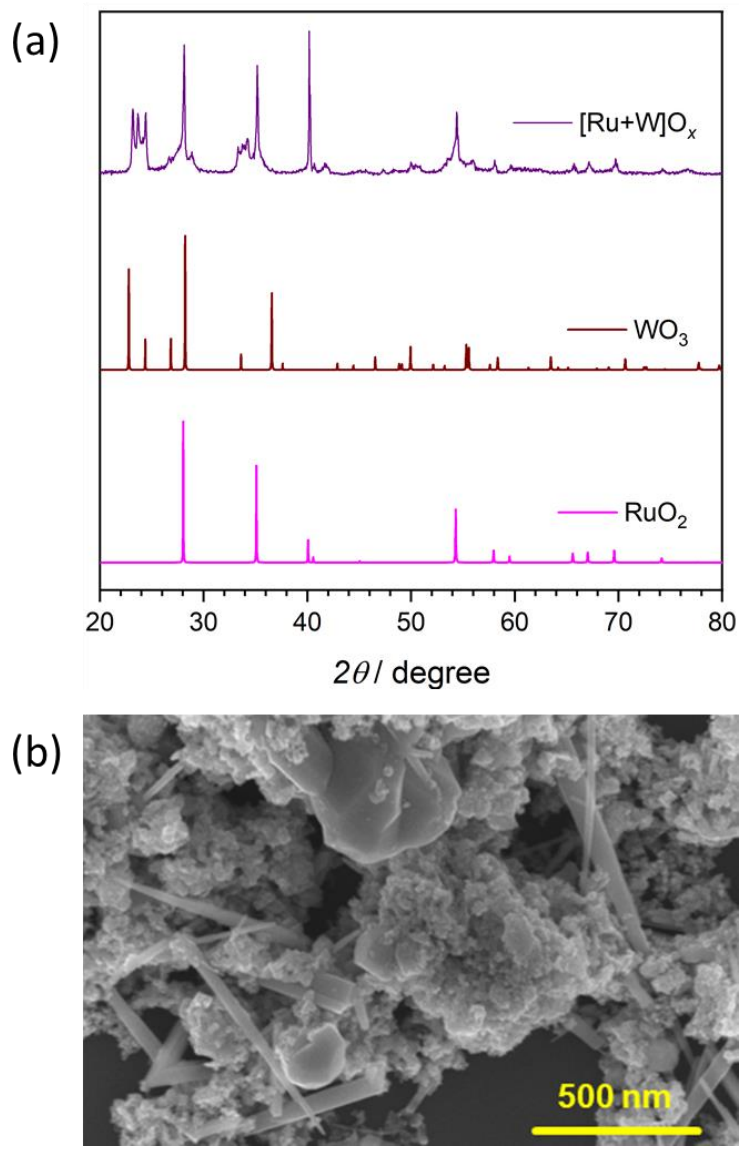

Figure S14. Physical characterisation of [Ru+W]O_x.

(a) X-ray diffraction pattern with peaks assigned to the RuO_2 (COD 1000058) and WO_3 (COD1004057) phases, and (b) SEM image recorded for [Ru+W]O_x synthesised using 0.6 mmol $(NH_4)_{10}H_2(W_2O_7)_6$ and calcination temperature of 600 °C.

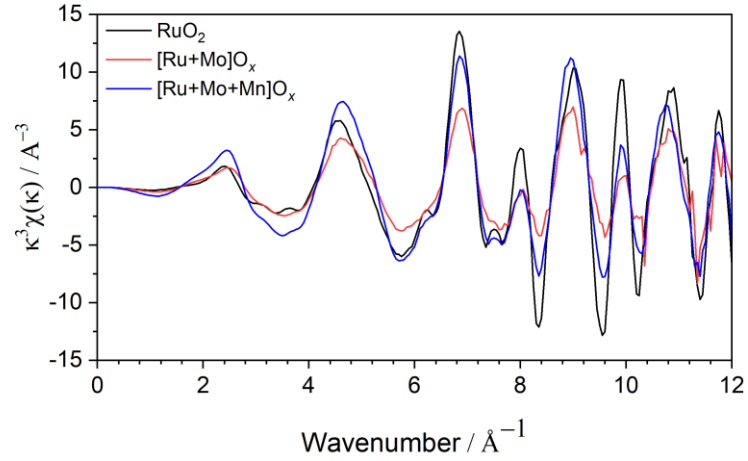

Figure S15. Ru K-edge EXAFS of the Ru- and Mo-based electrocatalysts.
Data were recorded for commercial RuO_2 (*black*), and for the freshly synthesised $[Ru+Mo]O_x$ (*red*) and $[Ru+Mo+Mn]O_x$ (*blue*) electrocatalysts.

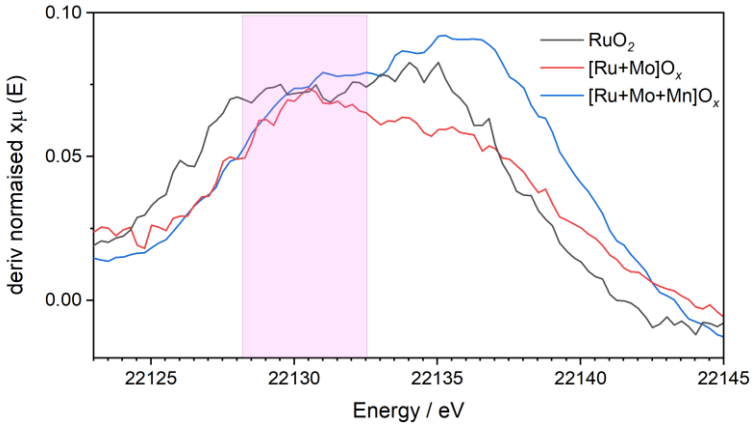

Figure S16. First derivative of Ru K-edge XANES for the Ru- and Mo-based electrocatalysts.
Data were recorded for commercial RuO_2 (*black*), and for the freshly synthesised $[Ru+Mo]O_x$ (*red*) and $[Ru+Mo+Mn]O_x$ (*blue*) electrocatalysts. Pink area highlights difference in the position of the rising edge for the composite samples as compared to RuO_2.

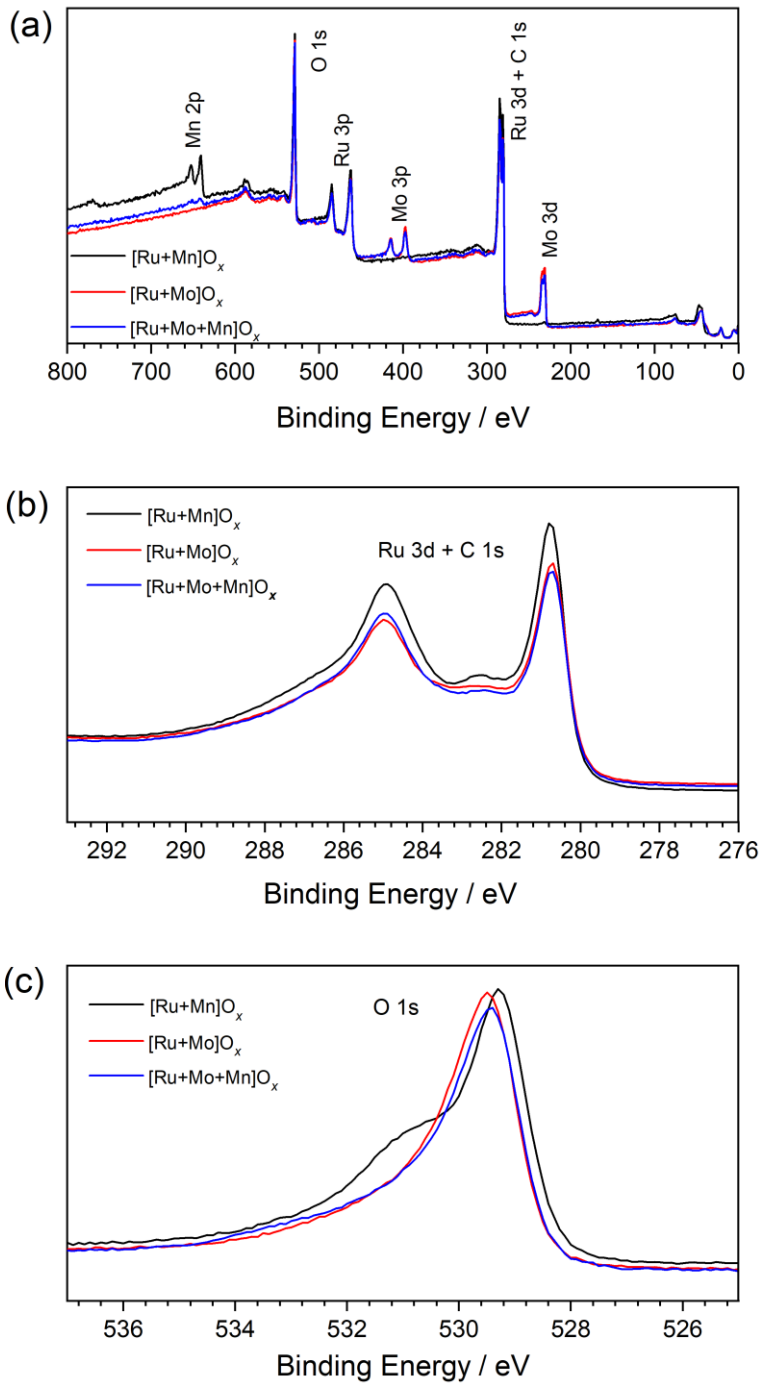

Figure S17. Supplementary XPS data for the Mn- and Mo-based composites.

(a) Survey, (b) Ru 3d + C 1s, and (c) O 1s spectra for the as-prepared [Ru+Mn]O_x (*black*), [Ru+Mo]O_x (*red*), and [Ru+Mo+Mn]O_x (*blue*) electrocatalysts.

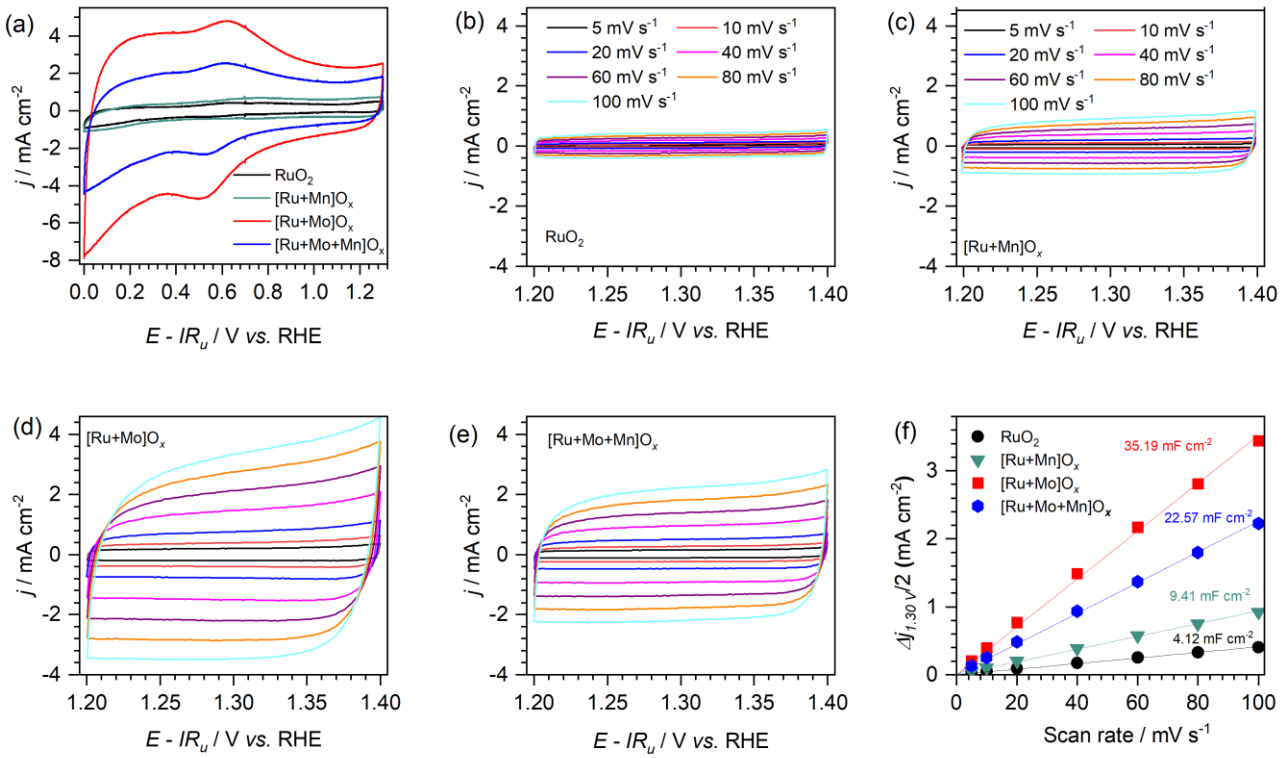

Figure S18. Active surface area measurements for the Ru, Mn and Mo-based catalysts.
(a) Cyclic voltammograms (v = 0.010 V s^{-1}; 5th quasi-stabilised scans) recorded for RuO_2 (*black*), [Ru+Mn]O_x (*teal*), [Ru+Mo]O_x (*red*), and [Ru+Mo+Mn]O_x (*blue*). (b-e) Cyclic voltammograms recorded at different scan rates shown in the figure for (b) RuO_2, (c) [Ru+Mn]O_x, (d) [Ru+Mo]O_x, and (e) [Ru+Mo+Mn]O_x. (f) Dependence of the capacitive currents on the potential scan rate derived from data in panels b-e (*symbols*) along with the linear fits (*lines*), which were used to calculate the *ECSA* values, for RuO_2 (*black*), [Ru+Mn]O_x (*teal*), [Ru+Mo]O_x (*red*), and [Ru+Mo+Mn]O_x (*blue*). Experiments were conducted using a GC electrode (0.20 cm^2) modified with 0.25 mg cm^{-2} of a catalyst in O_2-saturated, stirred (600 rpm) 0.5 M H_2SO_4 at 23 ± 2 °C. Currents are normalised to the geometric surface area of the electrode (0.20 cm^2); potentials were post-corrected for ohmic losses.

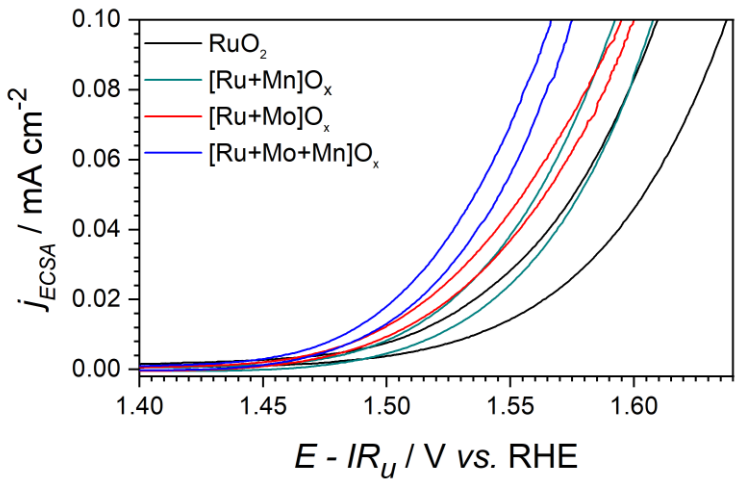

Figure S19. *ECSA*-specific OER catalytic activity of the Ru, Mn and Mo-based catalysts.
Data are presented as cyclic voltammograms (v = 0.010 V s^{-1}; 5th quasi-stabilised scans) normalised to the *ECSA* values summarised in **Figure 4**b (main text) recorded using a GC electrode (0.20 cm^2) functionalised with 0.25 mg cm^{-2} of RuO_2 (*black*), [Ru+Mn]O_x (*teal*), [Ru+Mo]O_x (*red*), and [Ru+Mo+Mn]O_x (*blue*). Experiments were undertaken in O_2-saturated, stirred (600 rpm) 0.5 M H_2SO_4 at 23 ± 2 °C. Potentials were post-corrected for ohmic losses.

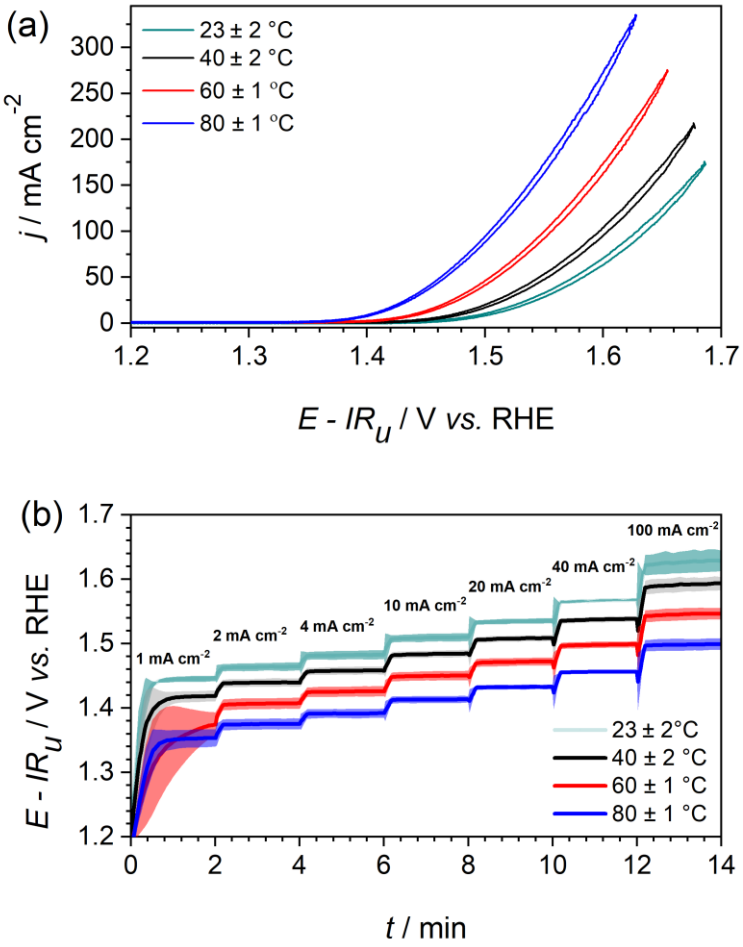

Figure S20. OER performance of [Ru+Mo+Mn]O_x at different temperatures.

(a) Cyclic voltammograms (v = 0.010 V s^{-1}; 5th quasi-stabilised scans), and (b) chronopotentiograms at different current densities (see figure) recorded for a Pt/Ti electrode functionalised with 0.25 mg cm^{-2} of [Ru+Mo+Mn]O_x at 23 ± 2 (*teal*), 40 ± 2 (*black*), 60 ± 1 (*red*), and 80 ± 1 °C (*blue*). Data in panel b are shown as mean (*curves*) ± standard deviation (*shading*) for tests of n = 3 independent samples. Experiments were undertaken in O_2-saturated, stirred (600 rpm) 0.5 M H_2SO_4. Currents are normalised to the geometric surface area of the electrode (0.25 cm^2); potentials were post-corrected for ohmic losses.

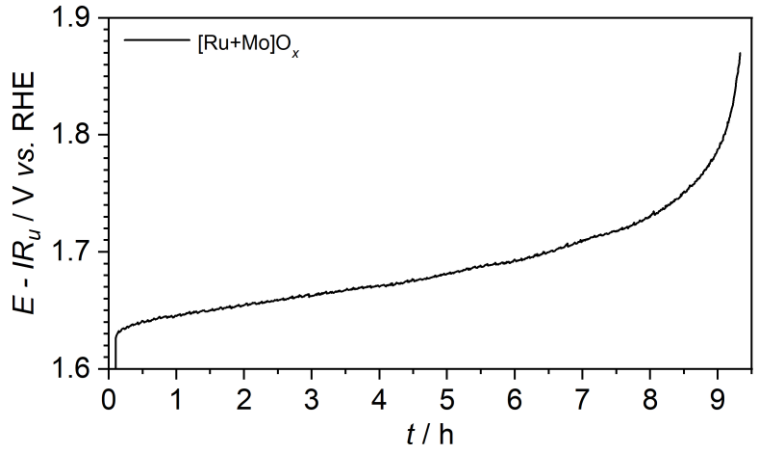

Figure S21. Stability test of [Ru+Mo]O_x.

Extended chronopotentiogram recorded for a Pt/Ti electrode functionalised with 0.20 mg cm^{-2} of [Ru+Mo]O_x at 100 mA cm^{-2} (per geometric surface area of the electrode; 0.25 cm^2) and 23 ± 2 °C in O_2-saturated, stirred (600 rpm) 0.5 M H_2SO_4. Potentials were post-corrected for ohmic losses.

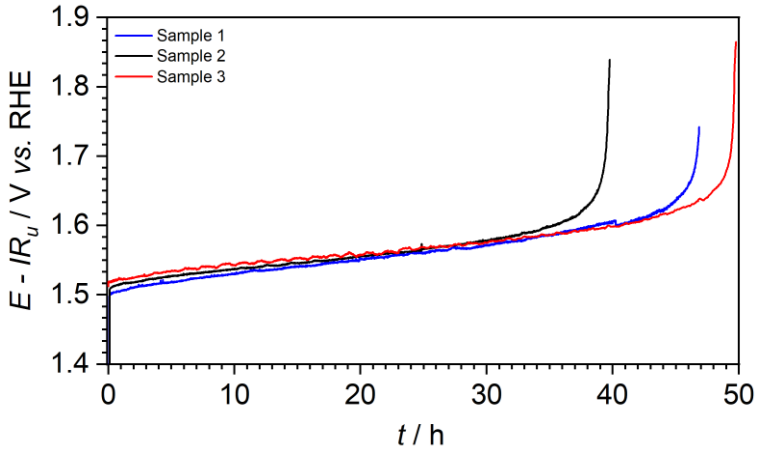

Figure S22. Reproducibility of the extended performance of [Ru+Mo+Mn]O_x.

Chronopotentiograms recorded for a Pt/Ti electrode functionalised with 0.20 mg cm^{-2} of [Ru+Mo+Mn]O_x at 100 mA cm^{-2} (per geometric surface area of the electrode; 0.25 cm^2) and 23 ± 2 °C in O_2-saturated, stirred (600 rpm) 0.5 M H_2SO_4. Data are shown for n = 3 independently synthesised samples. Potentials were post-corrected for ohmic losses.

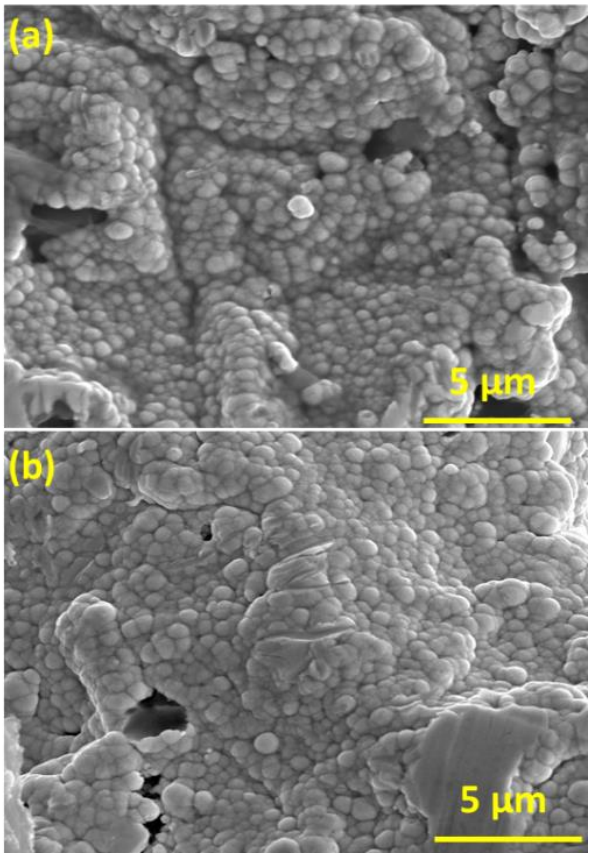

Figure S23. SEM images of [Ru+Mo+Mn]O_x/Pt/Ti before and after extended OER test.
SEM images of the electrode (0.25 mg cm^{-2} initial catalyst loading) (a) before and (b) after the 47 h galvanostatic stability test conducted at 100 mA cm^{-2} and 80 ± 1 °C shown in **Figure 6**a (main text).

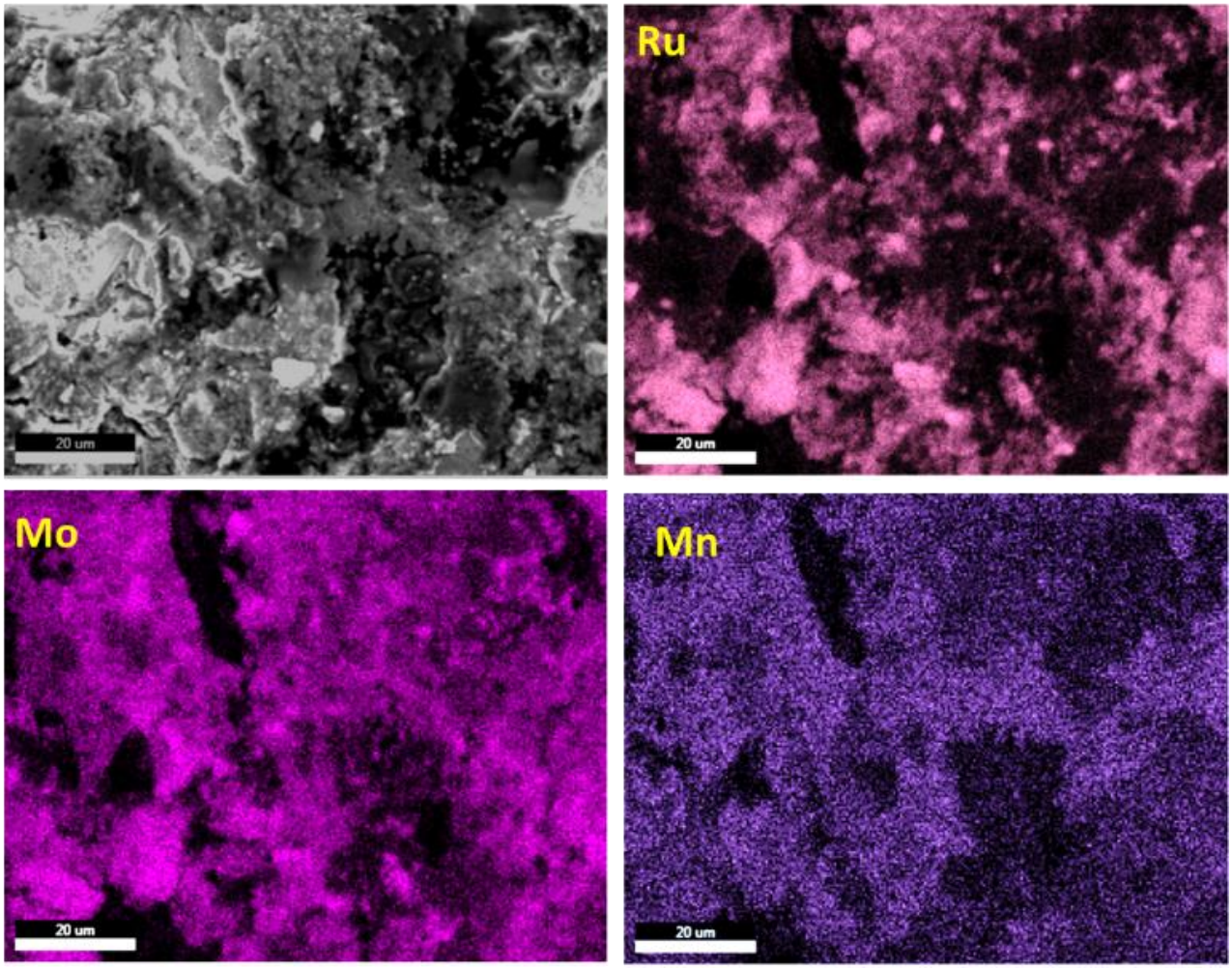

Figure S24. EDS mapping of [Ru+Mo+Mn]O_x/Pt/Ti after extended OER test.

SEM image and corresponding EDS elemental maps for Ru, Mo, and Mn recorded for the electrode (0.25 mg cm^{-2} initial catalyst loading) after the 47 h galvanostatic stability test conducted at 100 mA cm^{-2} and 80 ± 1 °C shown in **Figure 6**a (main text). Corresponding atomic ratios derived from the integrated maps are summarised in **Table S2**.

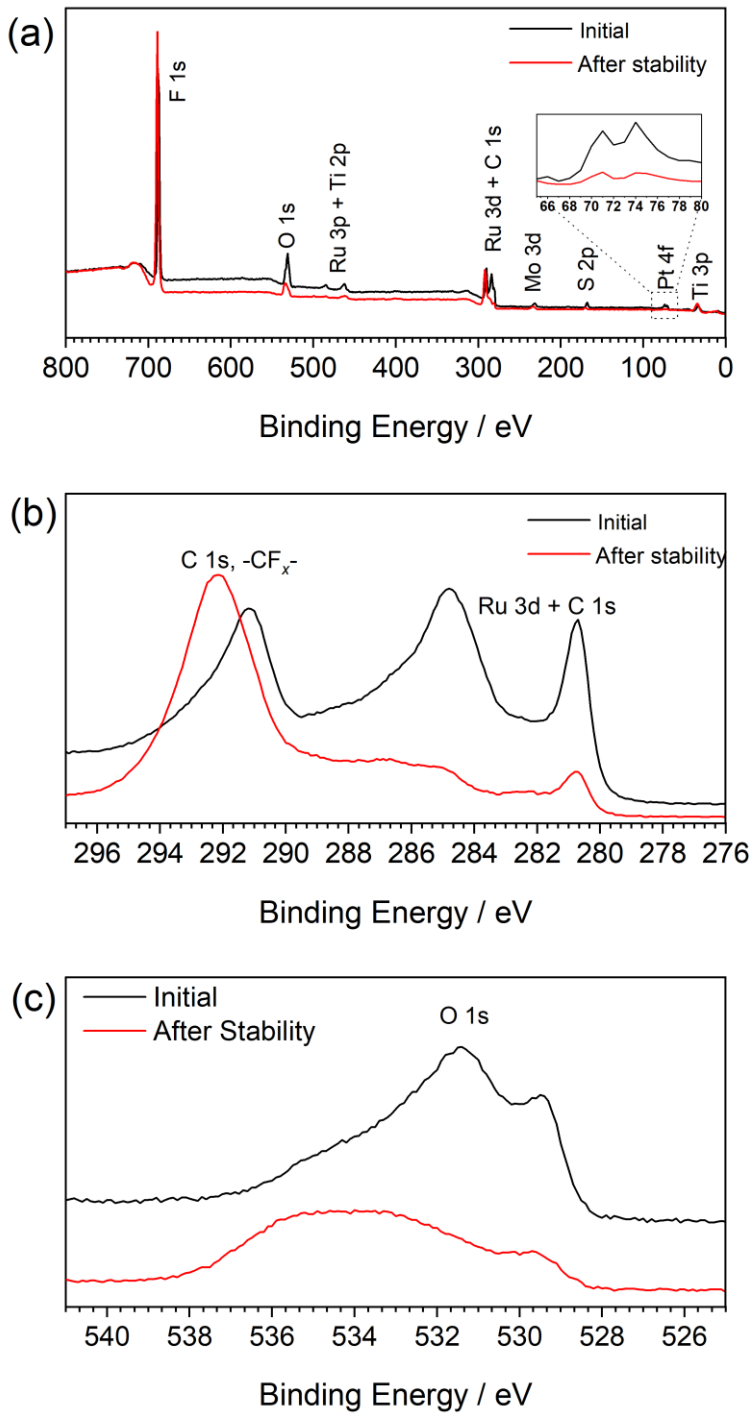

Figure S25. Supplementary XPS data for [Ru+Mo+Mn]O_x before and after extended OER test. (a) Survey (inset shows a magnified plot of the Pt 4f region), (b) Ru 3d + C 1s, and (c) O 1s spectra for the Pt/Ti electrodes functionalised with [Ru+Mo+Mn]O_x (0.25 mg cm^{-2} along with 40 wt.% Nafion ionomer) before (*black*) and after (*red*) the 47 h galvanostatic stability test conducted at 100 mA cm^{-2} and 80 ± 1 °C shown in **Figure 6**a (main text).

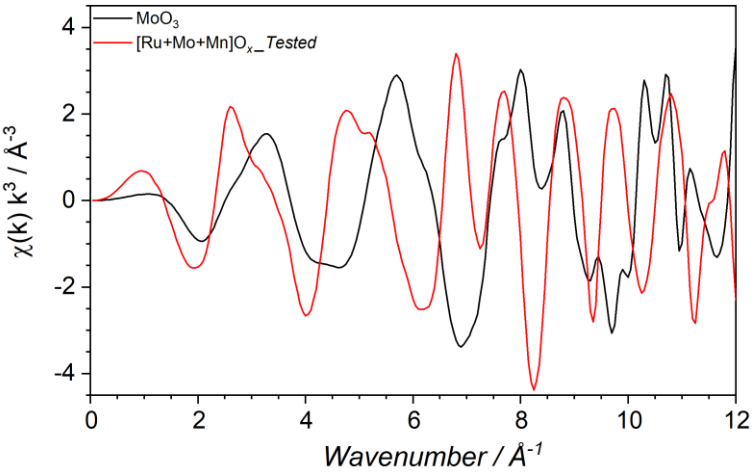

Figure S26. Mo K-edge EXAFS for [Ru+Mo+Mn]O_x after extended OER test.

Data were recorded for [Ru+Mo+Mn]O_x (*red*) after operation in 0.5 M H_2SO_4 at 100 mA cm^{-2} and 80 ± 1 °C for 50 h (corresponding electrochemical data are shown as *red* trace in **Figure S22**); data for the MoO_3 reference (*black*) are shown for comparison.

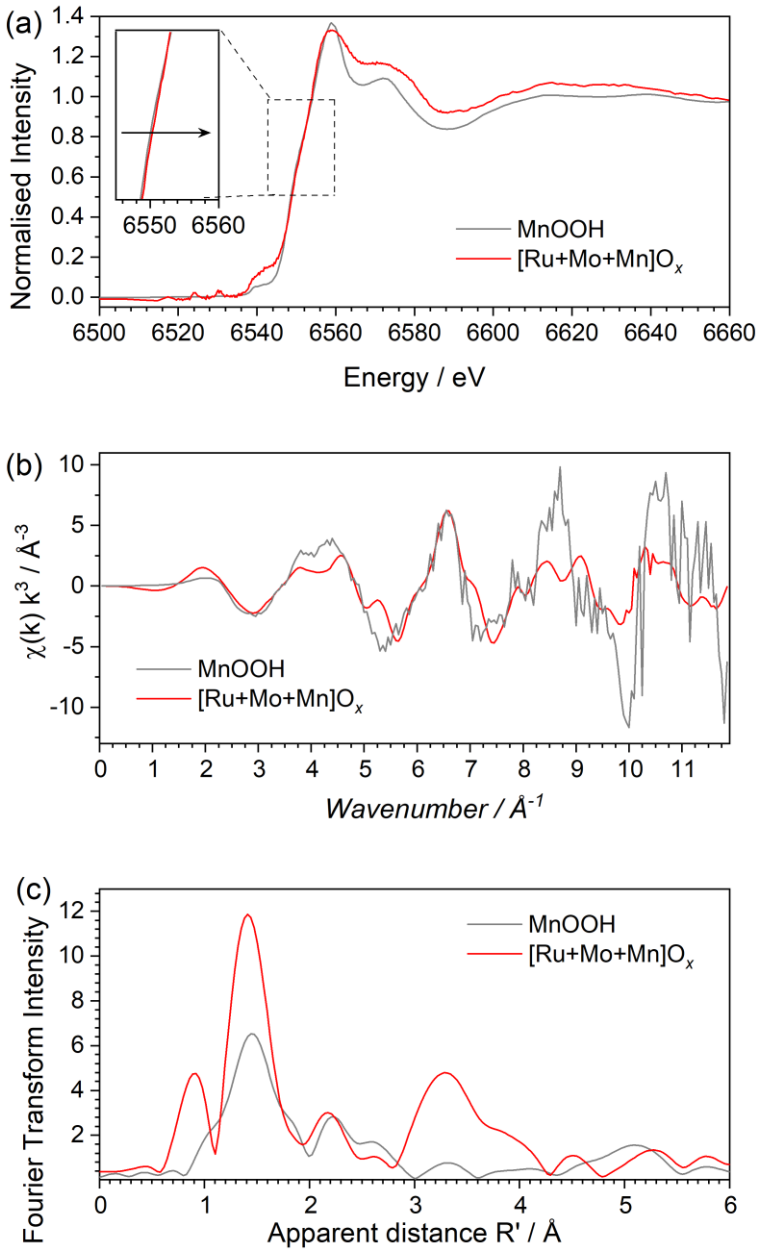

Figure S27. Mn K-edge XAS for [Ru+Mo+Mn]O_x after extended OER test.

(a) XANES, (b) EXAFS, and (c) FT EXAFS recorded for [Ru+Mo+Mn]O_x (*red*) compared to MnOOH reference (*grey*) after operation in 0.5 M H_2SO_4 at 100 mA cm^{-2} and 80 ± 1 °C for 50 h (corresponding electrochemical data are shown as *red* trace in **Figure S22**).

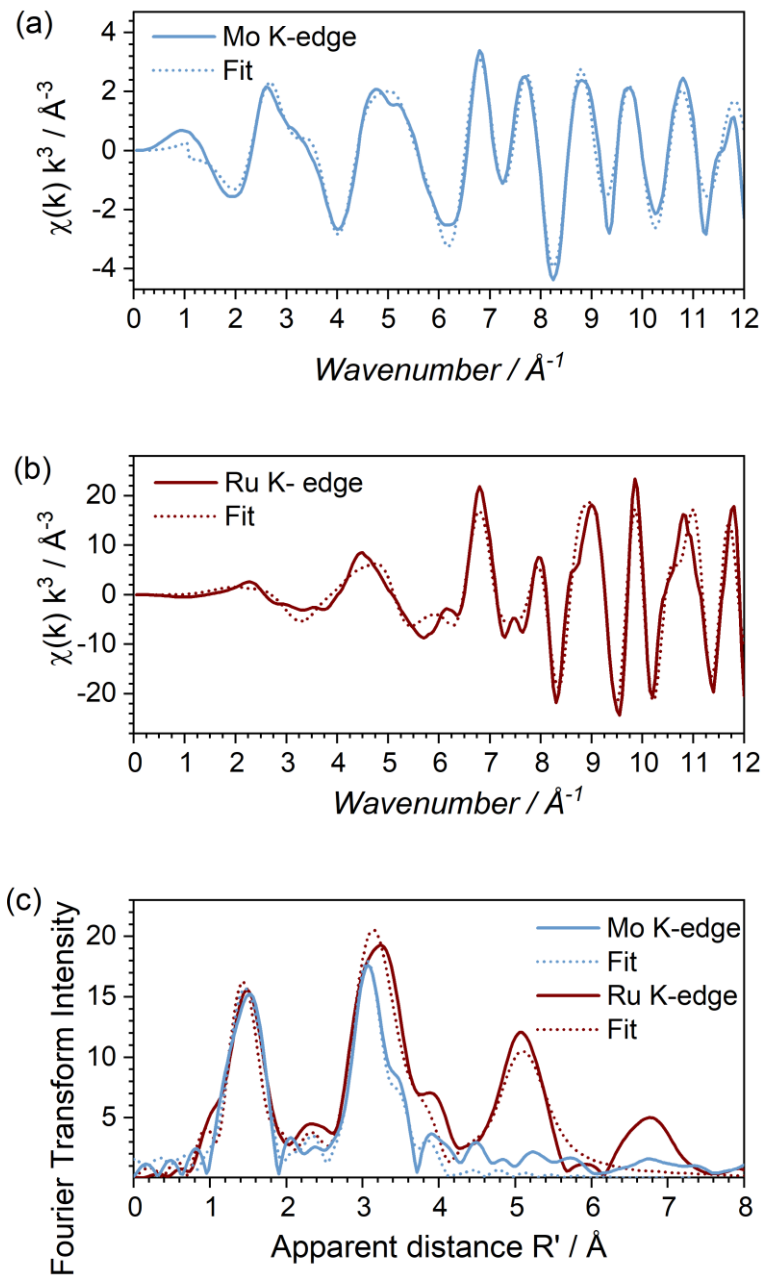

Figure S28. EXAFS and FT-EXAFS analysis of [Ru+Mo+Mn]O_x after extended OER test.
Experimental (*solid*) and simulated (*dotted*) (a-b) EXAFS and (c) FT EXAFS data at the Mo K- (*light blue*) and Ru K-edge (*wine*) for [Ru+Mo+Mn]O_x after operation in 0.5 M H_2SO_4 at 100 mA cm^{-2} and 80 ± 1 °C for 50 h (corresponding electrochemical data are shown as *red* trace in **Figure S22**). Fitting parameters are summarised in **Table S5**.

SUPPLEMENARY TABLES

Table S1. Performance of the selected Ru-based OER catalysts reported in literature.

Catalyst	Electrolyte	*T* / °C	Loading / mg cm^{-2}	Initial η_{10} / V [a]	Mass-normalised activity at η_{10}		Conditions of the stability test	Ref
					A g^{-1}_{cat}	A g^{-1}_{Ru}		
$RuO_2/(Co,Mn)_3O_4$	0.5 M H_2SO_4	23	2.9	0.270	9.2	370	24 h at 10 mA cm^{-2}	1
Co_3O_4 – RuCo@NC	0.5 M H_2SO_4	23	0.35	0.247	29	170	8 h at 10 mA cm^{-2}	2
$[Ru+Sb]O_x$	0.5 M H_2SO_4	80	0.22	0.340	45	99	8 days at 10 mA cm^{-2}	3
RuO_2/MoO_3	0.5 M H_2SO_4	23	0.56	0.247	1.3	1.5	300 h at 10 mA cm^{-2}	4
Co_3O_4/RuO_2-C	0.1 M $HClO_4$	23	1.0	0.170	10	370	45 h at 10 mA cm^{-2}	5
$RuCoO_x$	0.1 M $HClO_4$	23	2.4	0.200	4.3	230	100 h at 10 mA cm^{-2}	6
Ru/RuO_2-Co_3O_4	0.1 M $HClO_4$	23	7.1	0.226	1.4	7.0	10 h at 19 mA cm^{-2}	7
CoO_x/RuO_x-CC	0.5 M H_2SO_4	23	2.3	0.180	4.4	19	60 h at 10 mA cm^{-2}	8
$(Ru–W)O_x$	0.5 M H_2SO_4	23	2.0	0.170	5.0	not available	300 h at 10 mA cm^{-2}	9
$Ru_{0.6}W_{17.4}O_{49-\delta}$	0.5 M H_2SO_4	23	1.0	0.252	10	4200	45 h at 10 mA cm^{-2}	10
$Ru_5W_1O_x$	0.5 M H_2SO_4	23	1.5	0.235	6.7	18	550 h at 10 mA cm^{-2}	11
RuO_2–CeO_2–CC	0.5 M H_2SO_4	23	11	0.180	0.91	2.4	1000 h at 10 mA cm^{-2}	12
RuO_2/CeO_2@C	0.5 M H_2SO_4	23	1.0	0.170	10	340	100 h at 10 mA cm^{-2}	13
$Au/Pt/RuO_x$	0.1 M $HClO_4$	23	2.8	0.215	3.6	100	40 h at 10 mA cm^{-2}	14
NC/V_o·RuO_2/CNTs	0.5 M H_2SO_4	23	0.25	0.170	40	130	900 h at 10 mA cm^{-2}	15
Ru/RuS_2	0.5 M H_2SO_4	23	0.85	0.201	12	21	24 h at 10 mA cm^{-2}	16
$Ni-Ru/RuO_x$	0.5 M H_2SO_4	23	0.28	0.184	71	110	200 h at 20 mA cm^{-2}	17
$RuNi_2$/G-250	0.5 M H_2SO_4	23	0.32	0.227	31	54	24 h at 10 mA cm^{-2}	18
$Ru-RuO_2$/CNT	0.5 M H_2SO_4	23	N/A	0.180	not available	not available	11 h at 10 mA cm^{-2}	19
Ru/RuO_2/C	0.5 M H_2SO_4	23	0.11	0.276	136	not available	20 h at ~15 mA cm^{-2}	20
$Mn-RuO_2$	0.5 M H_2SO_4	25	0.28	0.158	36	50	10 h at ~10 mA cm^{-2}	21
$Mn_{0.73}Ru_{0.27}O_{2-\delta}$	0.5 M H_2SO_4	25	0.20	0.208	50	182	10 h at 10 mA cm^{-2}	22
$(Ru,Mn)_2O_3$-250	0.5 M H_2SO_4	25	0.28	0.168	36	161	40 h at 10 mA cm^{-2}	23
$12Ru/MnO_2$	0.1 M $HClO_4$	25	0.20	0.161	50	430	200 h at 10 mA cm^{-2}	24

[a] OER overpotential required to achieve the reaction rate of 10 mA cm^{-2} (per geometric surface area of the electrode).

Table S2. Composition of [Ru+Mo+Mn]O_x derived from different techniques.

Technique	Ru / at%	Mo / at%	Mn / at%
ICP-MS	59.2	24.0	16.8
EDS mapping			
as-prepared	70.3	24.4	5.3
tested [a]	71.0	25.	4.0
XPS			
as-prepared	66.8	29.6	3.6
tested [a]	83.8	overlap with S 2s [b]	5.1

[a] Experiments were undertaken using Pt/Ti electrodes modified with 0.25 mg cm^{-2} of the catalyst in 0.5 M H_2SO_4 at 100 mA cm^{-2} for 47 h (corresponding experimental data are shown in **Figure 6** in the main text). [b] Quantification of Mo is complicated by the overlap of the Mo 3d spectrum with the S 2s signals from the Nafion binder.

Table S3. Electrochemically active surface area of catalysts measured by voltammetry.

Electrocatalyst	Pseudocapacitance [a]		Total charge [b]	
	C_{dl} / F g^{-1}	*ECSA* / m^2 g^{-1}	*Q* / C g^1	A_{Ru} / m^2 g^{-1}
RuO_2	1.65	47.1	63.8	16.9
[Ru+Mn]O_x	3.78	108	104	27.4
[Ru+Mo]O_x	14.1	402	697	184
[Ru+Mo+Mn]O_x	9.03	258	373	98.7

[a] Derived from the pseudocapacitance measurements within a potential range of 1.2-1.4 V *vs.* RHE and a conversion factor of 0.035 mF cm^{-2}.[25] [b] Derived from the overall charge measured by voltammetry within the 0-1.3 V *vs.* RHE range and a conversion factor of 2643 cm^2 C^{-1}.[26] Voltammetric data were recorded using GC electrodes (0.2 cm^2) modified with 0.25 mg cm^{-2} of the catalyst and are exemplified in **Figure S18**.

Table S4. Corrosion of metals and ruthenium S-numbers for [Ru+Mo+Mn]O_x.[a]

Test conditions			Ru / at%	Mo / at%	Mn / at%	S_{Ru}-number
j / mA cm^{-2}	*T* / °C	*t* / h				
10	23 ± 2	100	6.1	18	6.1	1.4×10^5
100	23 ± 2	18	17	20	5.6	9.0×10^4
100	80 ± 1	24	7.7	32	12	2.6×10^5
100	80 ± 1	50	17	37	23	2.5×10^5

[a] Data are presented as at.% with respect to the initial amount of metals loaded on a Pt/Ti electrode (initial catalyst loading 0.25 mg cm^{-2}) and were derived from the ICP-MS analysis of the 0.5 M H_2SO_4 electrolyte solution before and after OER tests under different conditions defined in the table

Table S5. Mo K-edge EXAFS fitting parameters for [Ru+Mo+Mn]O_x.[a]

Atomic Pair	Number	Distance (XRD)	Distance (EXAFS)	Debye Waller (σ^2)
Mo-O	1	(1.73)[27]	1.65(0.02)	0.012(5)
	5	(1.96)	(1.95)	0.015(3)
Mo ..Ru/Mo	2	3.13 (N=8, RuO_2)[28]	(3.33)	0.0136(2)
Mo ..Ru/Mo	8	3.44 (N=2, RuO_2)[28]	3.23(18)	0.0003(1)
Mo ..O	4	3.45(N=4)	3.53(4)	0.008(6)
Mo .. group of O	4/16/2	4.05/4.12/4.28	3.7/3.77/3.92	0.0065(2)
Mo ..Ru/Mo	2	3.92	4.28(13)	0.0065(12)

[a] Corresponding experimental and simulated data are shown in **Figure S28**.

REFERENCES

1. S. Niu, X.-P. Kong, S. Li, Y. Zhang, J. Wu, W. Zhao and P. Xu, *Applied Catalysis B: Environmental*, 2021, **297**, 120442.
2. Z. Fan, J. Jiang, L. Ai, Z. Shao and S. Liu, *ACS applied materials & interfaces*, 2019, **11**, 47894-47903.
3. S. Luke, M. Chatti, A. Yadav, B. V. Kerr, J. Kangsabanik, T. Williams, P. V. Cherepanov, B. Johannessen, A. Tanksale and D. R. MacFarlane, *Journal of Materials Chemistry A*, 2021, **9**, 27468-27484.
4. W. Gou, S. Zhang, Y. Wang, X. Tan, L. Liao, Z. Qi, M. Xie, Y. Ma, Y. Su and Y. Qu, *Energy & Environmental Science*, 2024, **17**, 6755-6765.
5. F. Zhou, J. Chen, Y. Yang, X. Ke, X. Liu, L. Zhang, J. Li, H. Jin, S. Wang and Y. Li, *Applied Surface Science*, 2023, **641**, 158508.
6. W. Zhu, F. Yao, K. Cheng, M. Zhao, C.-J. Yang, C.-L. Dong, Q. Hong, Q. Jiang, Z. Wang and H. Liang, *Journal of the American Chemical Society*, 2023, **145**, 17995-18006.
7. T. Wang, Z. Li, H. Jang, M. G. Kim, Q. Qin and X. Liu, *ACS Sustainable Chemistry & Engineering*, 2023, **11**, 5155-5163.
8. L. Deng, S. Liu, D. Liu, Y. M. Chang, L. Li, C. Li, Y. Sun, F. Hu, H. Y. Chen and H. Pan, *Small*, 2023, **19**, 2302238.
9. L. Deng, S. F. Hung, Z. Y. Lin, Y. Zhang, C. Zhang, Y. Hao, S. Liu, C. H. Kuo, H. Y. Chen and J. Peng, *Advanced Materials*, 2023, **35**, 2305939.
10. X. Wang, H. Jang, S. Liu, Z. Li, X. Zhao, Y. Chen, M. G. Kim, Q. Qin and X. Liu, *Advanced Energy Materials*, 2023, **13**, 2301673.
11. Y. Wen, C. Liu, R. Huang, H. Zhang, X. Li, F. P. García de Arquer, Z. Liu, Y. Li and B. Zhang, *Nature Communications*, 2022, **13**, 4871.
12. H. Song, X. Yong, G. I. Waterhouse, J. Yu, H. Wang, J. Cai, Z. Tang, B. Yang, J. Chang and S. Lu, *ACS Catalysis*, 2024, **14**, 3298-3307.
13. Y. Wu, R. Yao, K. Zhang, Q. Zhao, J. Li and G. Liu, *Chemical Engineering Journal*, 2024, **479**, 147939.
14. T. Kwon, H. Yang, M. Jun, T. Kim, J. Joo, J. Kim, H. Baik, J. Y. Kim and K. Lee, *Journal of Materials Chemistry A*, 2021, **9**, 14352-14362.
15. H. Yan, Z. Jiang, B. Deng, Y. Wang and Z. J. Jiang, *Advanced Energy Materials*, 2023, **13**, 2300152.
16. J. Zhu, Y. Guo, F. Liu, H. Xu, L. Gong, W. Shi, D. Chen, P. Wang, Y. Yang and C. Zhang, *Angewandte Chemie*, 2021, **133**, 12436-12442.
17. A. M. Harzandi, S. Shadman, A. S. Nissimagoudar, D. Y. Kim, H. D. Lim, J. H. Lee, M. G. Kim, H. Y. Jeong, Y. Kim and K. S. Kim, *Advanced Energy Materials*, 2021, **11**, 2003448.
18. X. Cui, P. Ren, C. Ma, J. Zhao, R. Chen, S. Chen, N. P. Rajan, H. Li, L. Yu and Z. Tian, *Advanced Materials*, 2020, **32**, 1908126.
19. M. Zhang, J. Chen, H. Li, P. Cai, Y. Li and Z. Wen, *Nano Energy*, 2019, **61**, 576-583.
20. J.-L. Chen, S.-Y. Feng, C.-J. Lu and J.-F. Huang, *Chemical Engineering Journal*, 2023, **468**, 143761.
21. S. Chen, H. Huang, P. Jiang, K. Yang, J. Diao, S. Gong, S. Liu, M. Huang, H. Wang and Q. Chen, *Acs Catalysis*, 2019, **10**, 1152-1160.
22. K. Wang, Y. Wang, B. Yang, Z. Li, X. Qin, Q. Zhang, L. Lei, M. Qiu, G. Wu and Y. Hou, *Energy & Environmental Science*, 2022, **15**, 2356-2365.
23. Y. Qin, B. Cao, X.-Y. Zhou, Z. Xiao, H. Zhou, Z. Zhao, Y. Weng, J. Lv, Y. Liu and Y.-B. He, *Nano Energy*, 2023, **115**, 108727.
24. C. Lin, J.-L. Li, X. Li, S. Yang, W. Luo, Y. Zhang, S.-H. Kim, D.-H. Kim, S. S. Shinde and Y.-F. Li, *Nature catalysis*, 2021, **4**, 1012-1023.

25. C. C. McCrory, S. Jung, J. C. Peters and T. F. Jaramillo, *Journal of the American Chemical Society*, 2013, **135**, 16977-16987.
26. R. Savinell, R. Zeller and J. Adams, *Journal of the Electrochemical Society*, 1990, **137**, 489.
27. H. Yang, R. Jenkins, R. Thompson, R. Downs, S. Evans and E. Bloch, *American Mineralogist*, 2012, **97**, 197-202.
28. I. J. Davidson and J. Greedan, *Journal of Solid State Chemistry*, 1984, **51**, 104-117.